bioRxiv preprint doi: https://doi.org/10.1101/2022.06.23.497409; this version posted June 25, 2022. The copyright holder for this preprint (which was not certified by peer review) is the author/funder, who has granted bioRxiv a license to display the preprint in perpetuity. It is made available under aCC-BY-NC-ND 4.0 International license.

Rearrangements of Piezo1 blade domains correlate with pore opening

Alper D. Ozkan, Tharaka D. Wijerathne, Tina Gettas, and Jérôme J. Lacroix*

Department of Basic Medical Sciences, College of Osteopathic Medicine of the Pacific, Western University of Health Sciences, 309 E. Second St, Pomona, CA 91766

***corresponding**
Email: jlacroix@westernu.edu

Abstract

Mechanosensitive Piezo channels are anticipated to open their pore by flattening of large transmembrane domains called blades. Yet, direct experimental evidence for the coupling between blade motions and pore opening remains sparse. Here, we report unambiguous correlations between flow-induced Piezo1 opening and fluorimetric signals from conformation-sensitive probes genetically-inserted at two blade locations, one extracellular distal and the other intracellular proximal. Inhibition of gating motions near the pore with disulfide crosslinks reduced the amplitude of fluorescence signals from the most distal probe, consistent with long-range pore-blade conformational coupling. Interestingly, both probes remained fluorimetrically silent when Piezo1 opening was evoked with hypotonic shocks, cellular indentations, or application of the chemical activator Yoda1. This work provides direct experimental evidence that the Piezo1 blades act as mechanosensory domains and suggests that different mechanical stimuli activate Piezo1 through distinct mechanotransduction pathways.

bioRxiv preprint doi: https://doi.org/10.1101/2022.06.23.497409; this version posted June 25, 2022. The copyright holder for this preprint (which was not certified by peer review) is the author/funder, who has granted bioRxiv a license to display the preprint in perpetuity. It is made available under aCC-BY-NC-ND 4.0 International license.

Introduction

Rapid cellular adaptation to mechanical stress is vital for all organisms. This task is commonly achieved by mechanosensitive ion channels, membrane proteins that open transmembrane ion-permeant pores in response to mechanical stimuli. In eukaryotes, Piezo proteins act as general mechanotransducers capable of sensing forces produced by fluid displacement (*1-5*), tactile stimuli (*6-10*), tissue distension (*11-17*) and musculoskeletal movements (*18-22*). Piezo channels participate to an astonishing diversity of biological processes, including neurosensory functions (*23*), development (*24-30*), cell volume homeostasis (*31-33*), inflammation (*34-40*), and wound healing (*41*).

Cryo-electron microscopy (cryo-EM) structures of mammalian Piezo channels (Piezo1 and Piezo2) solved in detergent micelles show a common homotrimeric architecture with a central cation-selective pore, topped by an extracellular cap domain and surrounded by three large (> 2000 amino acids) peripheral domains arranged like the blades of a propeller, or the arms of a triskelion (*42-46*). The blades consist of a linear arrangement of nine conserved transmembrane bundles of α-helices, called Piezo repeats A to I (or transmembrane helical units 1-9). In these structures, the three blades extend from the pore in a helical manner, giving the trimeric channel a bowl shape. This non-planar structure is thought to correspond to a non-conducting conformation populated in absence of mechanical stimulus.

Piezo1 sense an astonishing variety of mechanical stimuli, including mechanical deformations of the lipid bilayer (*47-49*), hydrostatic pressure (*50*), fluid shear stress (*1, 2, 5, 25, 26, 51-53*), myosin-mediated traction forces (*54*), hypotonic shocks (*49, 55, 56*), substrate displacement (*57*) and cellular indentations (*58*). Structural studies have established that the Piezo1 blades flatten in response to mechanical deformations of the surrounding membrane. For instance, electron micrographs (*59*) and cryo-EM structures (*60*) of Piezo1 reconstituted into small proteoliposomes show that the curvature mismatch between channel and liposome is sufficient to deform the blades. In addition, high-speed atomic force microscopy kymographs indicate that Piezo1 elastically flattens when a compressive force is applied perpendicular to the lipid bilayer (*59*). Piezo1 blade flattening was computationally induced by membrane stretching (*61*) or by the curvature mismatch imposed by virtually clustering adjacent channels (*62*). In both computational studies, blade flattening led to an open state, supporting the prevailing view that mechanical forces open Piezo channels by flattening their blades.

In spite of these efforts, a direct experimental correlation between blade motions and pore opening has not yet been firmly established. Indeed, although a flattened Piezo1 conformation has been captured by cryo-EM, the moderate resolution in the pore region did not enable to unambiguously link this conformation to a functional state (*60*). In addition, although a correlation between applied force and blade flattening has been established (*59*), the functional consequences of blade flattening remain unclear. Blade mutations alter sensitivity to mechanical stimuli in Piezo1 and Piezo2, but a structure-function interpretation of these phenotypes remain difficult to parse (*63-65*). Although crosslinking the blade to the cap fully abolishes mechanically-induced currents in Piezo1, it is unclear whether this loss of mechanical sensitivity is caused by reduced mobility of the cap, the blade, or both domains (*66*). Last, although magnetic actuation of nanoparticles attached to the blade modulates macroscopic Piezo1 kinetics, it did not significantly alter open probability in absence of mechanical force (*67*).

bioRxiv preprint doi: https://doi.org/10.1101/2022.06.23.497409; this version posted June 25, 2022. The copyright holder for this preprint (which was not certified by peer review) is the author/funder, who has granted bioRxiv a license to display the preprint in perpetuity. It is made available under aCC-BY-NC-ND 4.0 International license.

Here, we use a fluorimetric approach to track force-induced rearrangements of the Piezo1 blade in real-time while the functional state of the pore is assessed using calcium imaging. Using flow-induced shear stress as a mechanical stimulus, we establish unambiguous temporal correlations between Piezo1 opening and robust unquenching of fluorescence probes genetically inserted at two blade positions separated by ~1500 residues in the primary amino acid sequence and by ~20 nm in the tridimentional Piezo1 structure, consistent with global blade rearrangement. We next explore how pharmacological treatments and structural perturbations known to affect Piezo1 function modulate the fluorimetric response of each probe. Remarkably, we discovered that disulfide crosslinks known to abolish Piezo1 opening by mechanical stimuli also reduces the amplitude of flow-dependent signals from the distal probe (*66*), showing long-distance blade-pore coupling. Interestingly, neither probe responds to hypotonic shocks or mechanical indentations, despite the effectiveness of these stimuli to open Piezo1 as assessed with calcium imaging and electrophysiology. Our data provides conclusive evidence that the Piezo1 blade operates as a mechanosensory domain and suggests that flow-induced shear stress elicit conformational rearrangements distinct from those produced by other stimuli.

Results

Generation of Piezo1-cpGFP constructs

Site-specific fluorimetry constitutes a powerful approach to capture real-time conformational changes associated with functional transitions in voltage-gated and ligand-gated ion channels (*68, 69*). Here, we adapt this technique for the first time to a mechanosensitive Piezo channel. Because the chemical attachment of dyes to protein of interests often requires inefficient and non-specific labeling steps, we used circular permuted green fluorescent proteins (cpGFP) as genetically encodable conformation-sensitive probes. Near the site of cpGFP insertion, stimulus-induced local conformational changes in the host protein often lead to quenching or unquenching of cpGFP fluorescence (*70*), a phenomenon that has inspired the rapid development of numerous genetically-encoded fluorescent indicators (*71-75*). We cloned cpGFP from the voltage-indicator ASAP1 (*76*) and inserted it at the carboxyl end of mPiezo1 residues 86, 300 and 1591, three positions previously shown to tolerate proteinogenic modifications with no major alterations of channel function (**Figure 1A**) (*47, 55, 67*). We also inserted cpGFP at residue 656, i.e. adjacent to an extracellular loop necessary for mechanical activation (*64*), and at residue 1299, i.e. at the distal end of a long intracellular beam anticipated to transmit force from the blade to the pore (*64, 77*).

These constructs, named 86, 300, 656, 1299 and 1591, were transfected into mechano-insensitive HEK293$^{\Delta PZ1}$ cells in which endogenous Piezo1 expression is abolished (*78*). We first determined the sensitivity of these constructs to the agonist Yoda1 using the red calcium indicator jRGECO1a and epifluorescence imaging (*79, 80*). Our data show that cells expressing wild-type (WT) mPiezo1, 86 or 1591 exhibit significantly higher calcium responses (maximal relative fluorescence changes, or $m\Delta F/F_0$) than a negative control (Kruskal-Wallis test with Dunn's test for multiple comparisons, p-values < 0.05), whereas other constructs yielded poor sensitivity to the agonist (**Figure 1B**). We electrophysiologically assessed the mechanical sensitivity of 86 and 1591 with cell-attached patch-clamp stretching and whole-

bioRxiv preprint doi: https://doi.org/10.1101/2022.06.23.497409; this version posted June 25, 2022. The copyright holder for this preprint (which was not certified by peer review) is the author/funder, who has granted bioRxiv a license to display the preprint in perpetuity. It is made available under aCC-BY-NC-ND 4.0 International license.

cell poking recordings (*81*). **Figure 1C-F** shows both stimuli elicit ionic currents with similar mechanical sensitivity and kinetics as in WT channels at both negative and positive voltages.

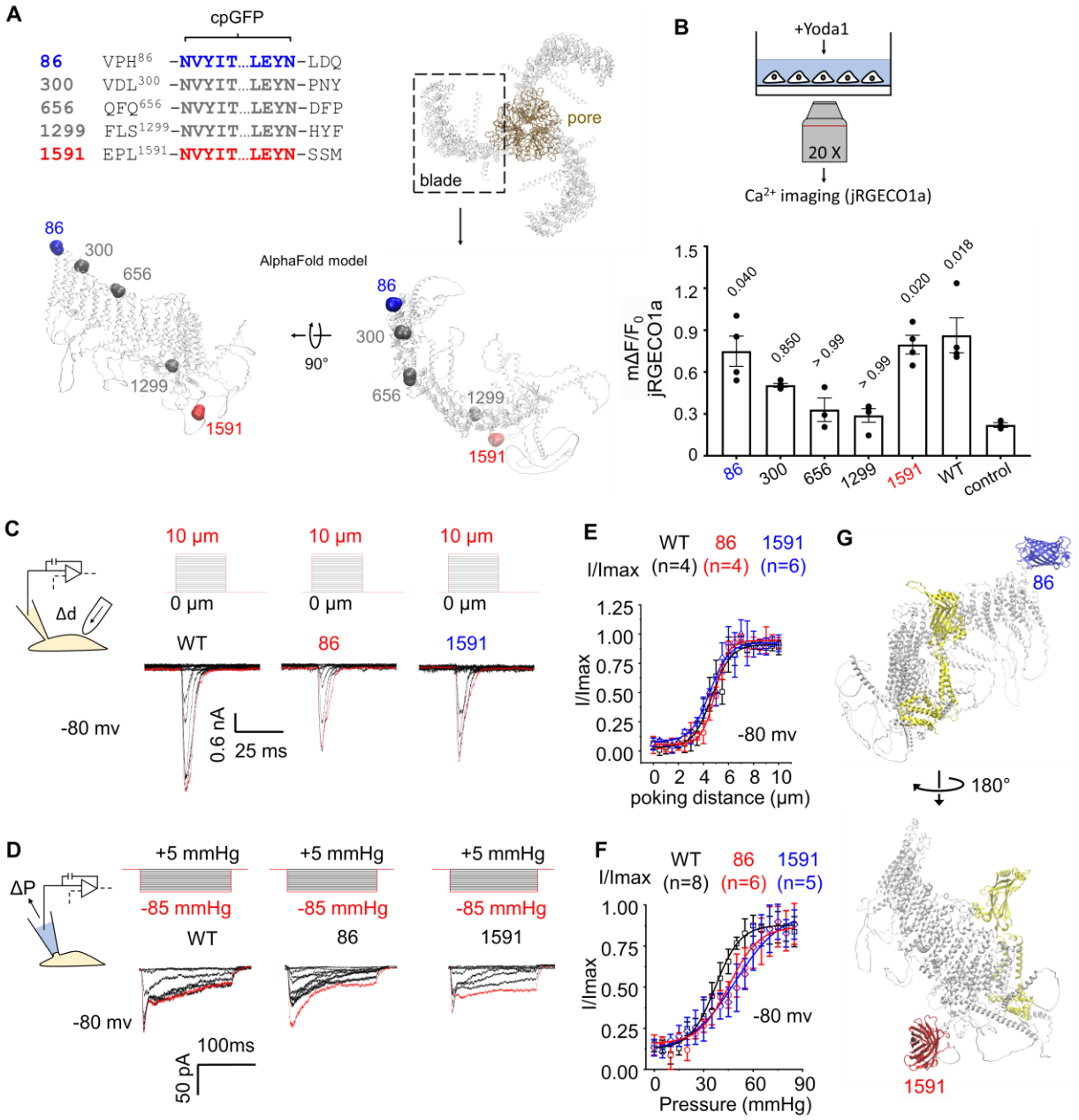

Figure 1. Insertion of cpGFP at two Piezo1 blade positions does not impair sensitivity to mechanical stimuli. (**A**) mPiezo1 sequence and structures identifying cpGFP insertion sites (Piezo1 structures PDB ID: 6B3R and AlphaFold). (**B**) Maximal calcium response (jRGECO1a) to acute incubation with 100 µM Yoda1 from HEK293T$^{\Delta PZ1}$ cells transfected or not with indicated Piezo1 constructs. Numbers above bars indicate p-values from Kruskal-Wallis test with Dunn's multiple comparisons. (**C-D**) Representative macroscopic current traces of 86, 1591 and WT Piezo1 in response to mechanical stretch (C, pipette pressure: +5 to -85 mmHg, duration: 200 ms, holding potential: -80 mV) and poking stimuli D, (indentation depth: 0 to 10 µm, duration: 100 ms, holding potential: -80 mV). (**E-F**) Relative peak current amplitude plotted as a function of pipette pressure (E) or poking displacement (F) in 86, 1591 and WT Piezo1. (**G**) Structural models of cpGFP inserted at positions 86 and 1591

bioRxiv preprint doi: https://doi.org/10.1101/2022.06.23.497409; this version posted June 25, 2022. The copyright holder for this preprint (which was not certified by peer review) is the author/funder, who has granted bioRxiv a license to display the preprint in perpetuity. It is made available under aCC-BY-NC-ND 4.0 International license.

created using the Molecular Operating Environment (MOE) software with the cpGFP structure obtained from PDB ID: 3o77 and the mPiezo1 structure from the AlphaFold structural model.

86 and 1591 fluorimetrically respond to shear stress

Having established that 86 and 1591 (**Figure 1G**) retain normal mechanosensitivity, we next ask whether these constructs produce fluorimetric responses to mechanical stimuli. We first seeded transfected cells into commercial closed-loop flow chambers mounted onto an epifluorescence microscope and applied calibrated amounts of shear stress by perfusing a saline solution (extracellular Hank's Balanced Saline Solution, or HBSS) using a computer-operated peristaltic or syringe pump (*71*) (**Figure 2A**).

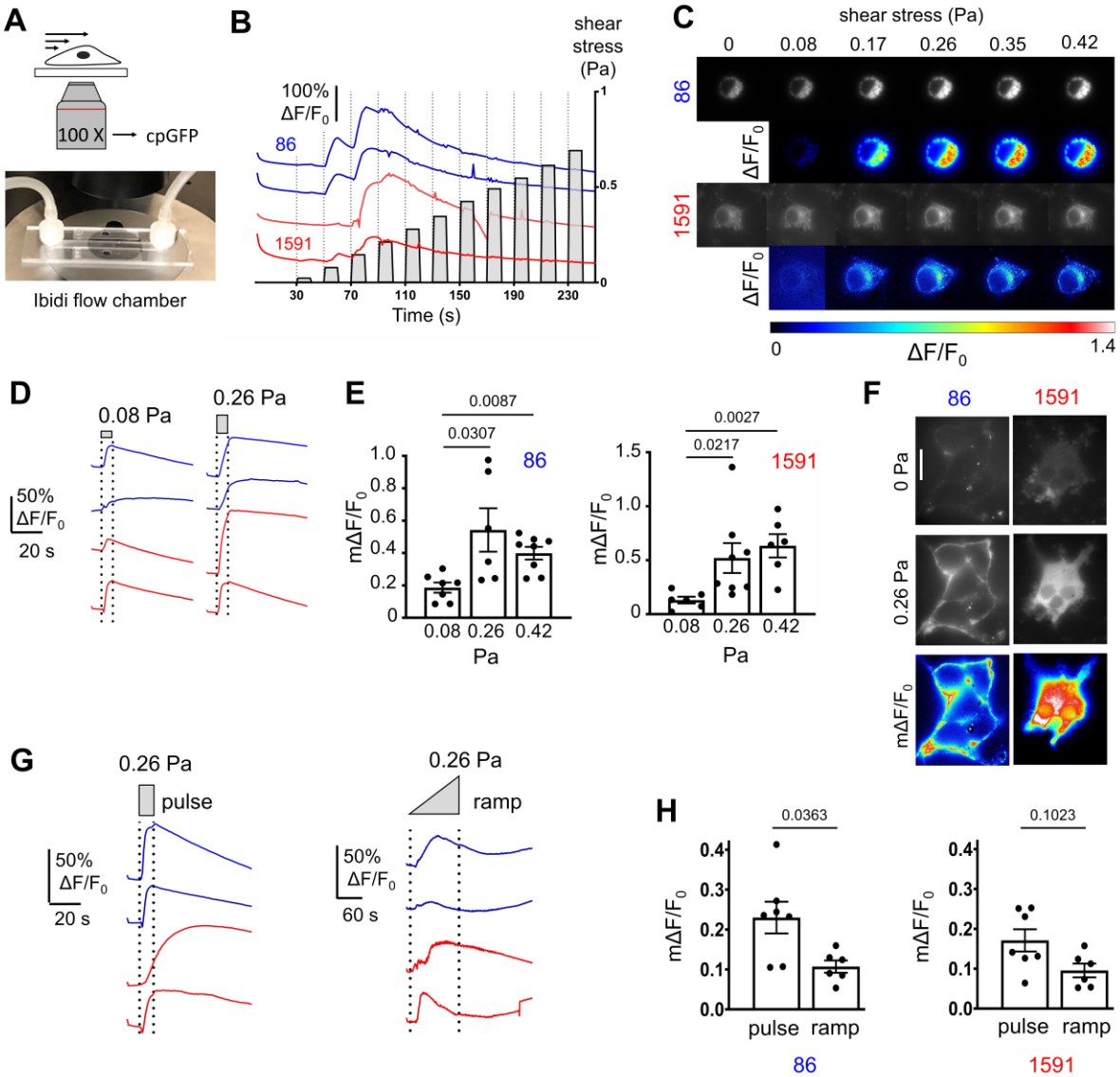

Figure 2. Flow stimuli induce robust fluorescent responses in both 86 and 1591. (**A**) Picture and schematic of our laminar shear stress protocol. (**B**) Representative fluorescence time-course of 86 and 1591 in response to shear stress stimulation applied in a series of 11 escalating pulses (pulse duration: 10 s, pulse magnitude: 0.022 – 0.691 Pa). (**C**) Representative epifluorescence images showing the time course of 86 and 1591 activation under conditions described in (B) and corresponding relative fluorescence changes ($\Delta F/F_0$). (**D**) Representative

bioRxiv preprint doi: https://doi.org/10.1101/2022.06.23.497409; this version posted June 25, 2022. The copyright holder for this preprint (which was not certified by peer review) is the author/funder, who has granted bioRxiv a license to display the preprint in perpetuity. It is made available under aCC-BY-NC-ND 4.0 International license.

fluorescence traces of 86 and 1591 activation in response to a single 10 s pulse of sub-saturating (0.08 Pa) or saturating (0.26 Pa) flow stimulus. (**E**) Bar graphs representing maximum fluorescence increase ($m\Delta F/F_0$) in 86 and 1591 exposed to a single 10 s pulse of 0.08, 0.26, or 0.42 Pa stimulus. (**F**) Representative epifluorescence images and $m\Delta F/F_0$ images of cells expressing 86 and 1591 and exposed to a single 10 s flow pulse of 0.26 Pa. (**G**) Comparison of fluorescence activation of 86 and 1591 in response to pulsed versus gradual application of shear stress. 0.26 Pa of shear stimulus was delivered either as a single 10 s pulse or a gradual ramp starting at 0 Pa and increasing linearly to 0.26 Pa over 120 s. (**H**) Bar graphs representing mΔF/F0 of 86 and 1591 under pulse and ramp conditions described in (G). Each point in box plots represents a single independent cell. Numbers above bars indicate p-values from Kruskal-Wallis test with Dunn's multiple comparisons. All constructs were expressed in HEK293T$^{\Delta PZ1}$ cells.

Figure 2B-C shows representative fluorescence time courses and epifluorescence images from cells expressing 86 and 1591 and exposed to a series of incrementally-increased shear stress pulses. Both 86 and 1591 produce robust and transient fluorescence increases (unquenching) at shear stress values as low as 0.1 Pa. Critically, we recently showed that flow stimuli up to 1 Pa fail to elicit fluorescence signals from two control membrane protein constructs in which cpGFP is inserted extracellularly (as in 86) or intracellularly (as in 1591) and measured using an identical experimental apparatus (*71*). This suggests that the robust unquenching of cpGFP inserted at positions 86 and 1591 occur as a response to backbone rearrangements of the Piezo1 blade.

Using individual pulses of fluid flow, we next show that $m\Delta F/F_0$ in 86 and 1591 tend to increase as the amplitude of the shear stress stimulus increases (**Figure 2D-F**). We also show that $m\Delta F/F_0$ emitted by 86 and 1591 tend to be lower when shear stress is gradually increased to 0.26 Pa over 120 s (ramp) as compared to when a 0.26 Pa shear stress pulse is rapidly applied for 10 s (**Figure 2G**). This suggests that the flow-induced membrane mechanical stress sensed by Piezo1 channels depends on the shear stress temporal gradient, an interpretation consistent with prior observations showing that flow-dependent endothelial mechanotransduction signaling depends on shear stress temporal gradient (*82*). The cpGFP signals in 86 and 1591 do not occur in absence of flow stimulation and decay faster with longer illumination exposures, a characteristic of photobleaching effects (data not shown).

Given the relatively low flow threshold for eliciting cpGFP signals in 86 and 1591, we wondered whether these signals correlate with pore opening or with pre-opening gating transitions. Calcium imaging experiments show that our standard 0.26 Pa flow pulse produces robust calcium signals but only in cells co-transfected with plasmids encoding WT mPiezo1, 86 or 1591, indicating that these flow-induced calcium responses depend on Piezo1 (**Figure 3A-B**). Dual-wavelength imaging further indicates a temporal correlation between the onset of cpGFP and jRGECO1a signals induced by flow in the same cells (**Figure 3C**).

bioRxiv preprint doi: https://doi.org/10.1101/2022.06.23.497409; this version posted June 25, 2022. The copyright holder for this preprint (which was not certified by peer review) is the author/funder, who has granted bioRxiv a license to display the preprint in perpetuity. It is made available under aCC-BY-NC-ND 4.0 International license.

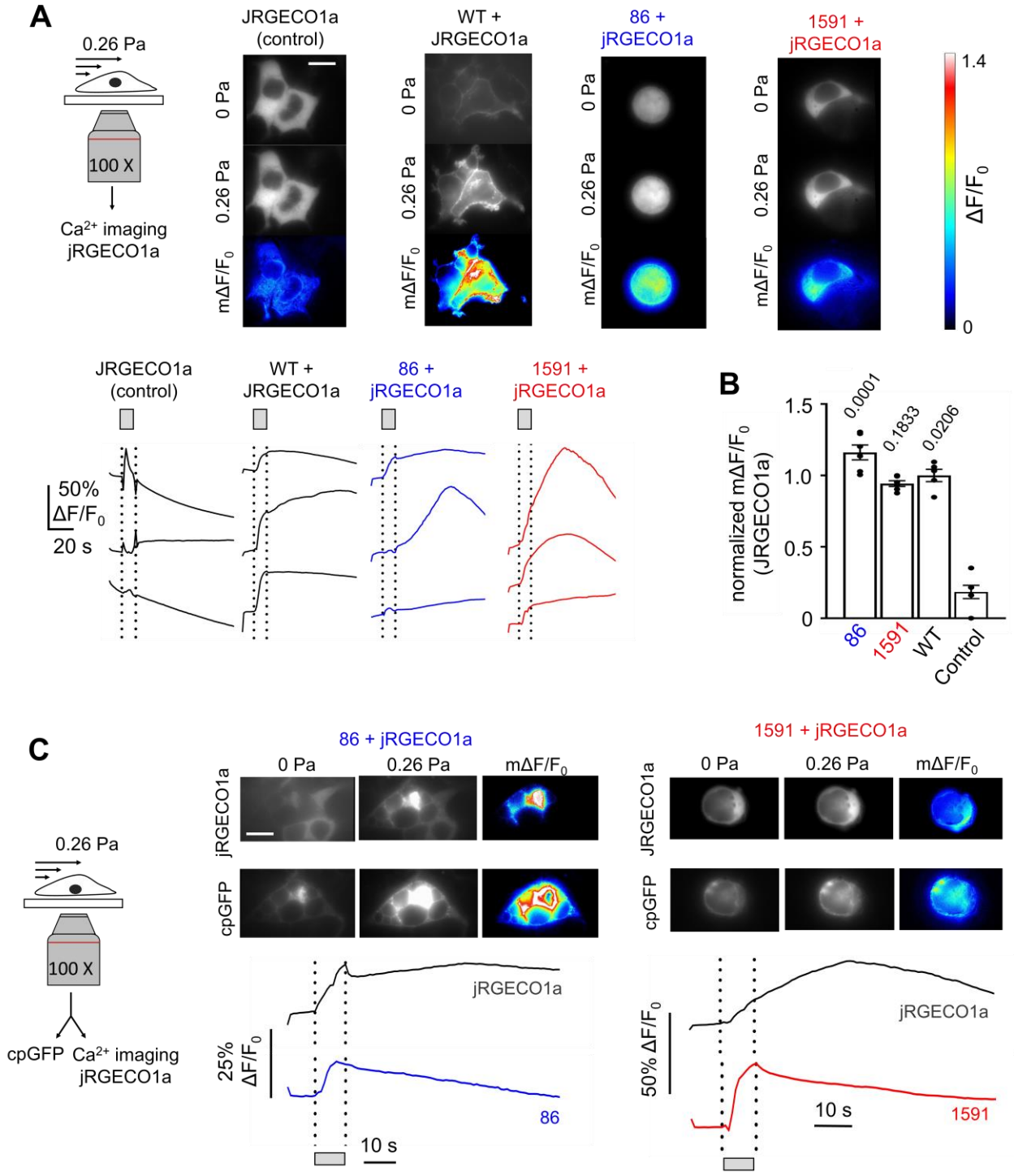

Figure 3. Shear stress-induced 86 and 1591 activation correlate with elevated cytosolic calcium levels. (A) Representative epifluorescence images and time traces of jRGECO1a in cells co-transfected or not with 86, 1591, or WT Piezo1, and exposed to a single 10 s pulse of 0.26 Pa shear stimulus. **(B)** Bar graphs representing $m\Delta F/F_0$ of jRGECO1a under co-transfection conditions and shear stimulation described in (A). **(C)** Representative dual fluorescence (jRGECO1a/cpGFP) images and time traces showing the concurrence of 86 or 1591 activation with cytosolic calcium entry. Each point in box plots represents a single independent cell. Numbers above each bar

bioRxiv preprint doi: https://doi.org/10.1101/2022.06.23.497409; this version posted June 25, 2022. The copyright holder for this preprint (which was not certified by peer review) is the author/funder, who has granted bioRxiv a license to display the preprint in perpetuity. It is made available under aCC-BY-NC-ND 4.0 International license.

indicate p-values from Kruskal-Wallis test with Dunn's multiple comparisons. All constructs were expressed in HEK293T-ΔPz1 cells.

Piezo1 channels rapidly inactivate upon sustained stimulation by various mechanical modalities, including poking, stretching, fluid shear stress and substrate deflection (*10, 26, 83*). To determine whether cpGFP unquenching correlate with open and/or inactivated states, we introduced pairs of mutations which individually slow down or accelerate Piezo1 inactivation. The first set of mutations, M2241R-R2482H, are murine homologs of human mutations M2225R and R2456H which individually slow down inactivation (*33, 84*). The second consists of L2475I-V2476I mutations which individually accelerate the rate of inactivation (*85*). We first confirmed that these phenotypes are conserved in 86 and 1591 using whole-cell poking recordings (**Figure 4A-B**). For both 86 and 1591, the intensity of flow-induced cpGFP signals was not significantly affected by the presence of either mutation pair (0.6274< p-values < 0.99) (**Figure 3C-E**), suggesting that both open and inactivated states promote cpGFP unquenching at both locations.

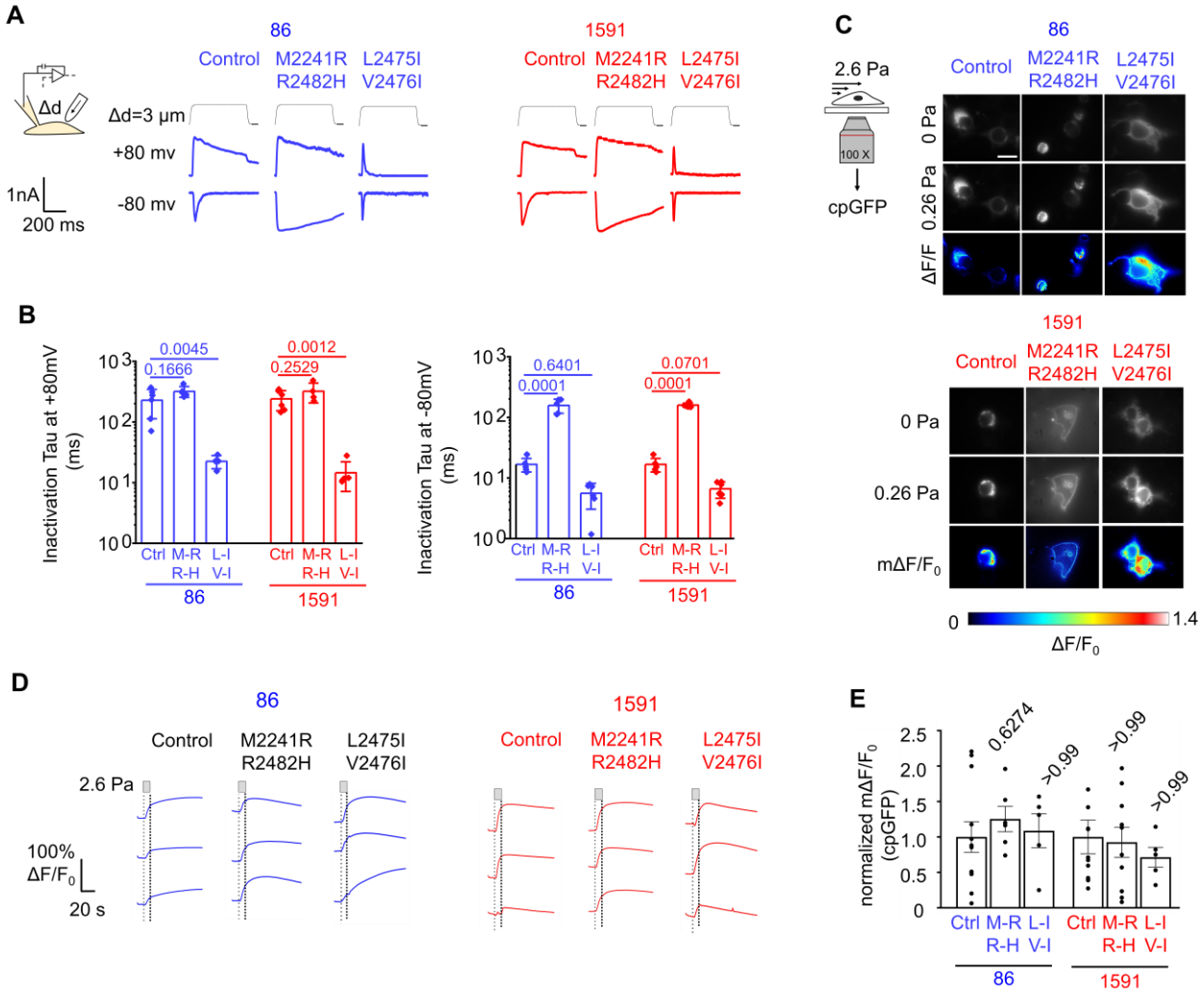

Figure 4. Shear stress-induced 86 and 1591 activation is insensitive to mutations that promote or inhibit inactivation. (**A**) Representative macroscopic poking-evoked current traces from cells expressing 86 or 1591

bioRxiv preprint doi: https://doi.org/10.1101/2022.06.23.497409; this version posted June 25, 2022. The copyright holder for this preprint (which was not certified by peer review) is the author/funder, who has granted bioRxiv a license to display the preprint in perpetuity. It is made available under aCC-BY-NC-ND 4.0 International license.

harboring point mutations that individually increase (L2475I/V2476I) or decrease (M2241R/R2482H) the rate of Piezo1 inactivation. Poking-induced currents from unmodified 86 and 1591 are provided as control. Cells were stimulated by 3 µm poking stimulus for 500 ms at a holding potential of -80 mV or +80 mV. (**B**) Inactivation Tau values of 86 and 1591 harboring or not the inactivation-modifying mutations under experimental conditions described in (A). (**C**) Representative epifluorescence responses of 86, 1591, and their inactivation mutations following exposure to a single 10 s pulse of 0.26 Pa flow stimulus. (**D-E**) Fluorescence traces and bar graphs representing mΔF/F0 values for the indicated constructs under experimental conditions described in (C). Each point in box plots represents a single independent cell. Numbers above each bar indicate p-values from Kruskal-Wallis test with Dunn's multiple comparisons. All constructs were expressed in HEK293T$^{\Delta PZ1}$ cells.

Pharmacological modulation of flow-induced cpGFP signals

We next tested the effect of amyloid beta fragment 1-40 (Aβ_{1-40}), GsMTx4 and cytochalasin D on shear-induced fluorescence response of 86 and 1591, as these pharmacological treatments were previously shown to inhibit Piezo1 activity (*53, 56, 86*).

As with mechanical stimuli, we also evaluated the effect of each treatment on Piezo1-dependent calcium responses. Although acute applications of Aβ_{1-40} peptides, at picomolar concentrations in monomeric forms or was reported to robustly inhibit flow-induced Piezo1-mediated calcium uptake (*53*), we observed no significant differences in flow-induced calcium responses in the presence or absence of 1 µM Aβ_{1-40} peptides in cells expressing WT mPiezo1, 86, or 1591 (Mann-Whitney U-test p-values > 0.99) (**Figure 5A-B**). This discrepancy may arise from differences in shear stress stimulation, as we use 10 s / ~0.26 Pa flow pulses as opposed to 10 ms / ~1.5 Pa flow pulses in the Maneshi et al. study (*53*). It is indeed possible that our 1000-fold longer flow duration promotes unbinding of amyloid peptides from the cell surface, precluding the proposed inhibitory effects. In line with these results, no differences were observed in cpGFP responses between control and treated groups (Mann-Whitney U-test p-values > 0.99) (**Figure 5C**).

By contrast, treatment of cells with 20 µM cytochalasin D robustly inhibited both calcium and cpGFP responses (**Figure 6A-C**), consistent with a role of the actin cytoskeleton in propagating fluid shear stress to Piezo1 channels. As a control, we treated cells with GsMTx4, an inhibitor of stretch-activated ion channels, including Piezo1 (*86*). As expected, GsMTx4 was effective to inhibit Piezo1-dependent flow-induced calcium entry (**Figure 6C**). Interestingly, the presence of GsMTx4 did not significantly alter the amplitude of flow-induced cpGFP signals at positions 86 and 1591 (**Figure 6A-B**).

bioRxiv preprint doi: https://doi.org/10.1101/2022.06.23.497409; this version posted June 25, 2022. The copyright holder for this preprint (which was not certified by peer review) is the author/funder, who has granted bioRxiv a license to display the preprint in perpetuity. It is made available under aCC-BY-NC-ND 4.0 International license.

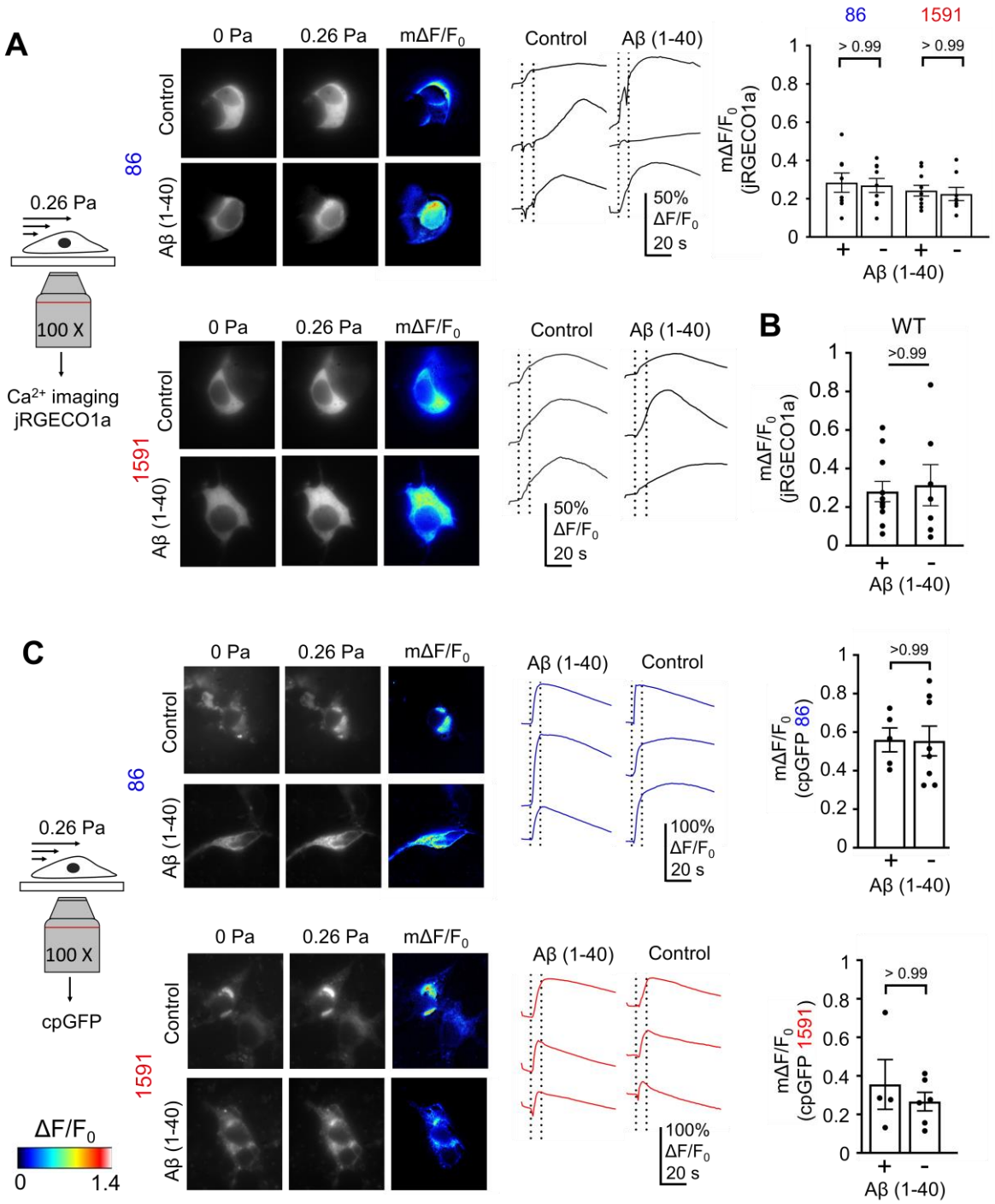

Figure 5. The presence of Aβ(1-40) peptide does not abolish flow-induced calcium signals and cpGFP activation. (**A-B**) Representative jRGECO1a fluorescence images, traces, and bar graphs of in cells co-transfected with 86, 1591, or WT mPiezo1 (B), exposed to a single 10 s pulse of 0.26 Pa stimulus in the presence or absence of 1 μM Aβ(1-40) peptide. (**C**) Representative cpGFP fluorescence images, traces, and bar graphs from cells expressing constructs 86 and 1591 and exposed to a single 10 s pulse of 0.26 Pa stimulus in the presence or absence of 1 μM Aβ(1-40) peptide. Each point in box plots represents a single independent cell. Numbers above each bar indicate p-values from Kruskal-Wallis test with Dunn's multiple comparisons. All constructs were expressed in HEK293T$^{\Delta PZ1}$ cells.

bioRxiv preprint doi: https://doi.org/10.1101/2022.06.23.497409; this version posted June 25, 2022. The copyright holder for this preprint (which was not certified by peer review) is the author/funder, who has granted bioRxiv a license to display the preprint in perpetuity. It is made available under aCC-BY-NC-ND 4.0 International license.

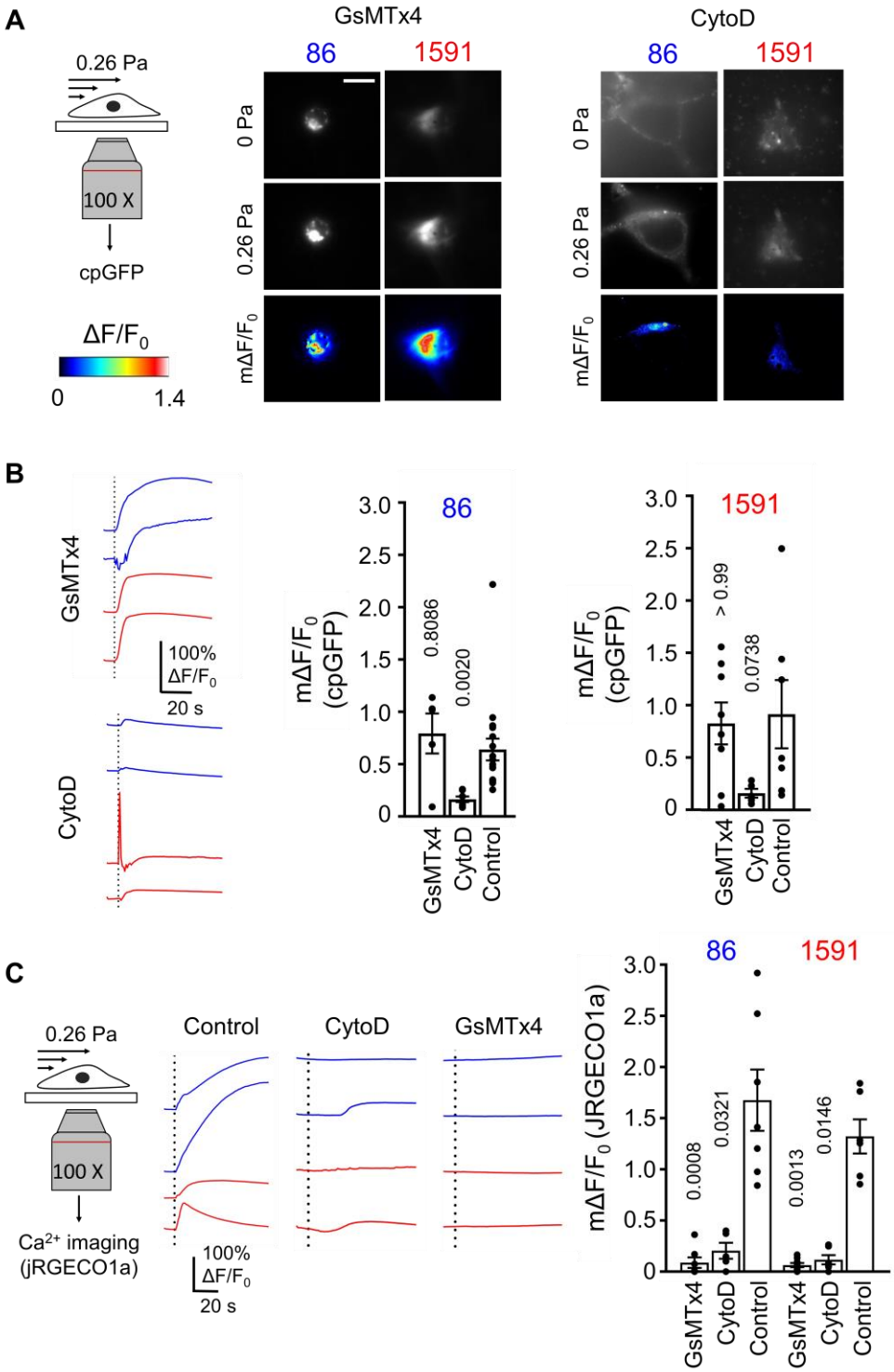

Figure 6. Flow-induced 86 and 1591 activation is inhibited by cytochalasin D but not GsMTx4. (**A**) Representative epifluorescence images of 86 and 1591, exposed to a single 10 s pulse of 0.26 Pa shear in the presence or absence of 5 μM GsMTx4 peptide or 20 μM cytochalasin D. (**B**) Representative fluorescence traces and bar graphs of 86 and 1591 treated as described in (A). (**C**) Representative fluorescence traces and bar graphs of jRGECO1a co-transfected with 86, 1591, or WT Piezo1, and treated as described in (A). Each point in

bioRxiv preprint doi: https://doi.org/10.1101/2022.06.23.497409; this version posted June 25, 2022. The copyright holder for this preprint (which was not certified by peer review) is the author/funder, who has granted bioRxiv a license to display the preprint in perpetuity. It is made available under aCC-BY-NC-ND 4.0 International license.

box plots represents a single independent cell. Numbers above each bar indicate p-values from Kruskal-Wallis test with Dunn's multiple comparisons. All constructs were expressed in HEK293T$^{\Delta PZ1}$ cells.

Proximal disulfide crosslinks reduce distal cpGFP signals

We next wondered whether inhibiting gating motions near the pore would retrogradely affect cpGFP signals from our probes. To test this hypothesis, we inserted proximal disulfide bridges previously shown to abolish poking-evoked Piezo1 currents in a DTT-dependent manner in both 86 and 1591 (*66*). We used R1762C/E2257C to crosslink the cap domain to an extracellular loop in Repeat B and A2328C/P2382C to crosslink residues within the cap. We measured flow-induced calcium responses in cells expressing these new constructs in presence or absence of 25 mM DTT in the extracellular solution. In both constructs, calcium responses were significantly larger in the presence of the reducing agent, confirming the inhibitory effect of cysteine substitutions (**Figure 7A**).

We next tested cpGFP activation in these new constructs in the presence or absence of DTT. The mean amplitude of flow-induced cpGFP signals from the distal probe 86 was about 2-fold larger in presence vs. absence of DTT for both tested cysteine pairs, an effect that was statistically significant for the construct harboring A2328C/P2382C (non-parametric Mann Whitney U-test p-value = 0.041) (**Figure 7B**). In contrast, flow-induced cpGFP signals from the two cysteine-modified 1591 constructs were conclusively unaffected by the presence of DTT (p-values > 0.99).

bioRxiv preprint doi: https://doi.org/10.1101/2022.06.23.497409; this version posted June 25, 2022. The copyright holder for this preprint (which was not certified by peer review) is the author/funder, who has granted bioRxiv a license to display the preprint in perpetuity. It is made available under aCC-BY-NC-ND 4.0 International license.

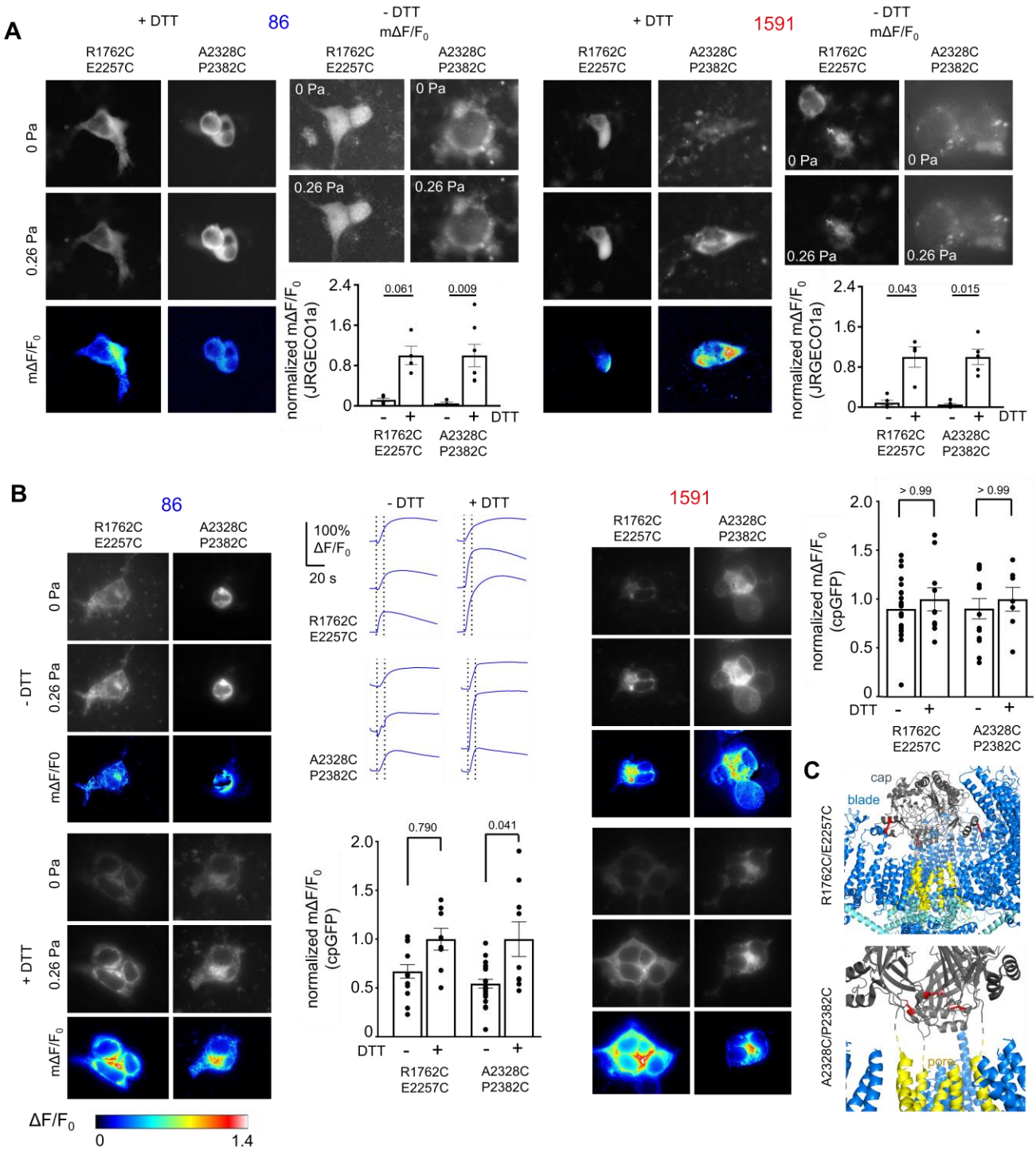

Figure 7. Long-distance conformational coupling between pore and blade domains. (**A**) Representative fluorescence images and bar graphs showing flow-induced calcium responses from 86 and 1591 constructs harboring a double cysteine mutation (R1762C/E2257C or A2328C/P2382C) in presence or absence of 25 mM DTT. (**B**) Representative fluorescence images, time-courses, and bar graphs showing flow-induced fluorimetric cpGFP responses from 86 and 1591 constructs harboring a double cysteine mutation (R1762C/E2257C or A2328C/P2382C) in presence or absence of 25 mM DTT. (**C**) Mutations R1762C/E2257C and A2328C/P2382C

bioRxiv preprint doi: https://doi.org/10.1101/2022.06.23.497409; this version posted June 25, 2022. The copyright holder for this preprint (which was not certified by peer review) is the author/funder, who has granted bioRxiv a license to display the preprint in perpetuity. It is made available under aCC-BY-NC-ND 4.0 International license.

are mapped onto the mPiezo1 structure (PDBID:6b3r). Numbers above each bar indicate p-values from Kruskal-Wallis test with Dunn's multiple comparisons. All constructs were expressed in HEK293TΔPZ1 cells.

86 and 1591 are fluorimetrically silent to osmotic swelling and mechanical indentation

We next sought to determine whether 86 and 1591 fluorimetrically respond to other mechanical stimuli. To this aim, we seeded transfected cells into standard culture dishes and exchanged extracellular HBSS with a hypotonic solution (~58 mOsmol L^{-1}). We first tested the effectiveness of this stimulus to activate WT and engineered channels. Our hypotonic stimulation produces robust Piezo1-dependent calcium signals (**Figure 8-BA**). However, this stimulus was unable to elicit cpGFP quenching or unquenching in 86 or 1591 (**Figure 8C-D**). Dual imaging experiments confirm that our hypotonic stimulation elicits robust calcium entry but no cpGFP fluorescence responses in the same cells (**Figure 8E**).

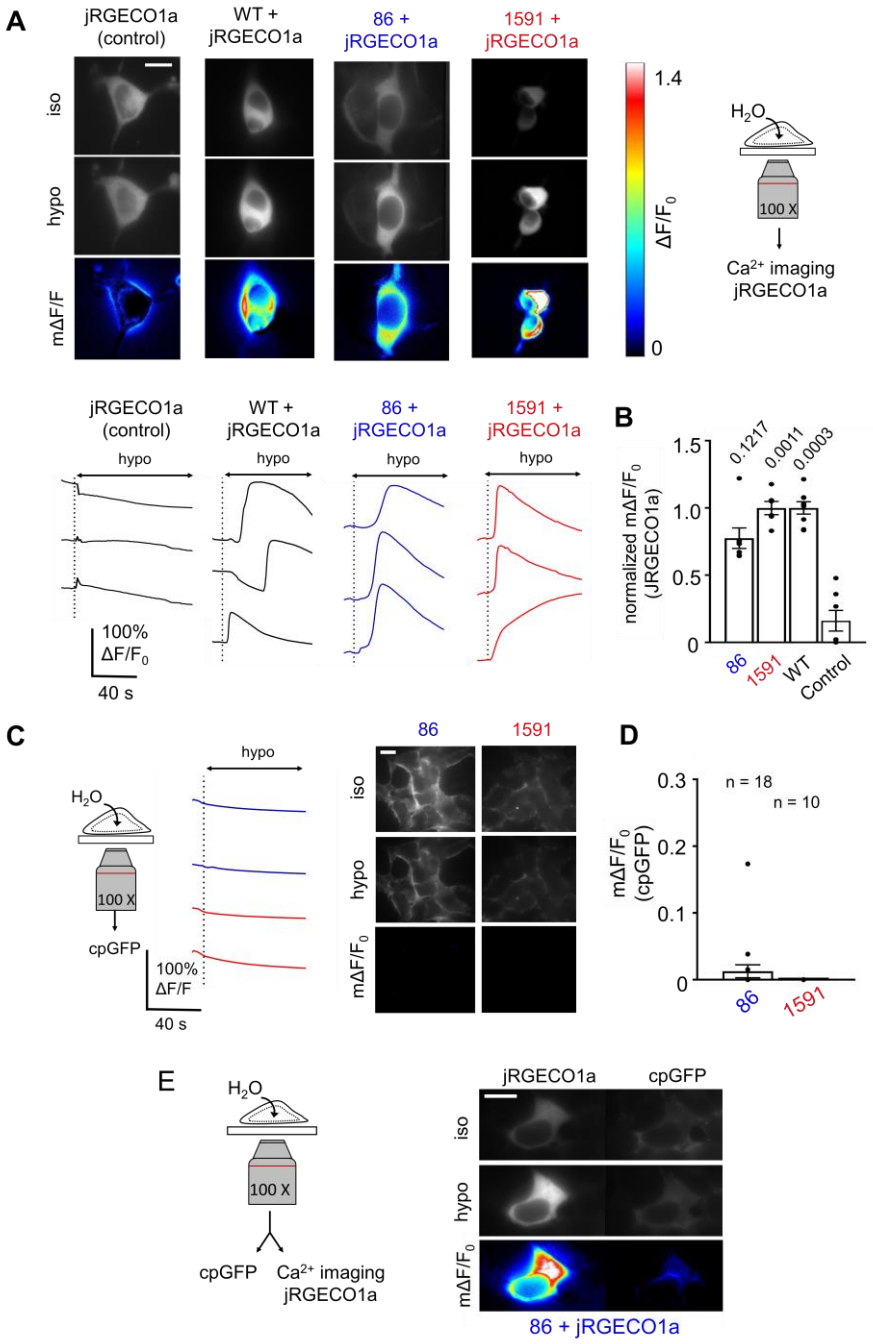

Figure 8. 86 and 1591 are fluorimetrically silent to hypotonic shocks. (**A**) Representative jRGECO1a fluorescence images and time traces in cells co-transfected with 86, 1591, WT Piezo1, or no Piezo1 (control), and exposed to a hypotonic solution (~58 mOsmol L-1) for 90 s. (**B**) Bar graphs plotting jRGECO1a $m\Delta F/F_0$ values from experiments described in (A) (normalized to WT mean value). (**C**) Representative cpGFP fluorescence images and time traces of 86 and 1591 following exposed to a hypotonic solution (~58 mOsmol L-1) for 90 s. (**D**) Bar graphs plotting $m\Delta F/F_0$ values of 86 and 1591 treated as described as (C). (**E**) Dual imaging showing activation of cpGFP 86 without concomitant activation of calcium signal. Numbers above each bar indicate p-values from Kruskal-Wallis test with Dunn's multiple comparisons. All constructs were expressed in HEK293T-ΔPz1 cells.

bioRxiv preprint doi: https://doi.org/10.1101/2022.06.23.497409; this version posted June 25, 2022. The copyright holder for this preprint (which was not certified by peer review) is the author/funder, who has granted bioRxiv a license to display the preprint in perpetuity. It is made available under aCC-BY-NC-ND 4.0 International license.

We next acutely indented cells using 5 µm poking / 1500 ms stimuli. Although these mechanical indentations evoke Piezo1-dependent calcium signals, no change in cpGFP fluorescence was observed in either 86 or 1591 (**Figure 9A-D)**. By contrast, cells showing visible physical damage upon poking produced sustained calcium signals but no cpGFP signals (data not shown).

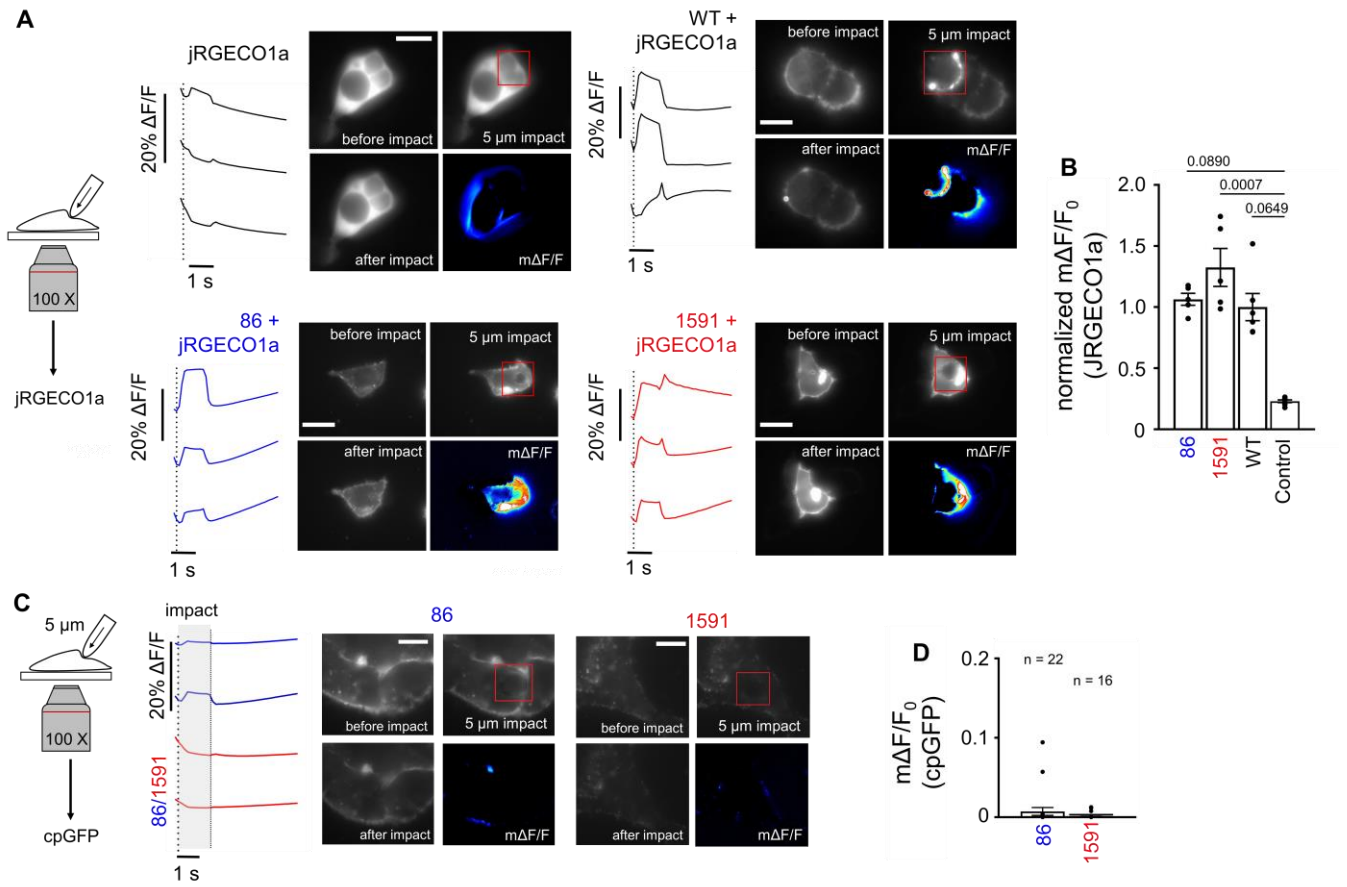

Figure 9. 86 and 1591 are fluorimetrically silent to poking stimulation. (**A**) Representative epifluorescence images and fluorescence traces of jRGECO1a co-transfected with 86, 1591, WT Piezo1, or no Piezo1 (control), and indented to a distance of 5 µm. (**B**) Bar graphs representing jRGECO1a m$\Delta F/F_0$ values from experiments described in (A) and normalized to mean WT value. (**C**) Representative epifluorescence images and fluorescence traces of cpGFP in cells expressing 86 and 1591 and indented to 5 µm. (**D**) Bar graphs representing m$\Delta F/F_0$ values of 86 and 1591 from experiments described in (C). Numbers above each bar indicate p-values from Kruskal-Wallis test with Dunn's multiple comparisons. All constructs were expressed in HEK293T$^{\Delta PZ1}$ cells.

Discussion

Most ion channels possess regulatory domains that control opening and closure of gates in the pore domain. Here, we test whether the Piezo1 blades act as regulatory domains sensitive to mechanical forces. To work as such, the Piezo1 blades must undergo conformational changes in response to mechanical stimuli and these rearrangements must correlate with modulation of open probability. Our data establishes unambiguous correlations between fluid flow stimulation, Piezo1-dependent calcium uptake, and local rearrangements of two distant blade locations, tracked using genetically-encoded

bioRxiv preprint doi: https://doi.org/10.1101/2022.06.23.497409; this version posted June 25, 2022. The copyright holder for this preprint (which was not certified by peer review) is the author/funder, who has granted bioRxiv a license to display the preprint in perpetuity. It is made available under aCC-BY-NC-ND 4.0 International license.

fluorimetric probes. Restricting protein flexibility near the pore region using inhibitory disulfide crosslinks further diminish cpGFP signal from the most distal probe near the N-terminus. These results constitute compelling experimental evidence supporting the notion that the Piezo blade domain acts as a mechanotransduction domain.

We further discovered that the integrity of the actin cytoskeleton is essential for flow-mediated activation of Piezo1. An actin-based mechanotransduction pathway has been recently proposed as a lipid-independent route for mechanical Piezo1 activation (*87*). It would be thus interesting to test whether other elements of this pathway, including Cadherin, β-catenin, and Vinculin are also necessary for flow-mediated Piezo1 activation.

Interestingly, our results show that GsMTx4 does not inhibit flow-induced cpGFP signals from neither one of our probes, despite the ability of this toxin to robustly inhibit Piezo1-dependent calcium uptakes. This suggests a pharmacological model in which GsMTx4 exert its inhibitory effects by means other than preventing the Piezo1 blades to rearrange upon mechanical stimulation. This view is consistent with a recent study showing that GsMTx4 inhibits a mechano-insensitive Piezo1 deletion mutant lacking the entire blade domain (*88*). On the other hand, GsMTx4 has been proposed to inhibit stretch-activated ion channels by interacting with the lipid bilayer (*89*), a mechanism which seems difficult to reconcile with these two independent experimental results. Future studies will be needed to discover the still elusive mechanism by which this toxin inhibits Piezos and other mechanosensitive channels.

The fact that our cpGFP probes 86 and 1591 do not respond to osmotic or poking stimuli that are otherwise effective at opening the channel pore does not necessarily mean that the local structure of these two blade locations remains unchanged during mechanical stimulation by swelling or poking. It is indeed possible that these local structures remain more or less static or that they undergo conformational rearrangements that are ineffective at modulating the fluorescence of the cpGFP inserts. Additionally, we cannot exclude the possibility that this differential fluorimetric sensitivity arises from the presence of cpGFP and would not occur in WT channels. However, we find this possibility unlikely, as this phenotype is observed independently at two blade locations that are separated by >1500 residues in the primary amino acid sequences and > 20 nm in the full-length Piezo1 subunit structure (predicted by AlphaFold) (*90*). The notion that different mechanical stimuli impart distinct local rearrangements of the blade is further consistent with previous experimental studies showing that certain blade mutations differentially affect the sensitivity of Piezo1 channel to mechanical stimuli such as poking and membrane stretch (*64, 77*).

bioRxiv preprint doi: https://doi.org/10.1101/2022.06.23.497409; this version posted June 25, 2022. The copyright holder for this preprint (which was not certified by peer review) is the author/funder, who has granted bioRxiv a license to display the preprint in perpetuity. It is made available under aCC-BY-NC-ND 4.0 International license.

Methods

Molecular cloning

The pCDNA3.1-mPiezo1 plasmid was generously donated by Dr. Ardèm Patapoutian (Scripps Research). cpGFP fragments were PCR-amplified from a pCDNA3.1-ASAP1 plasmid gifted by Dr. Francois Saint-Pierre (Baylor College of Medicine and Rice University) and inserted to desired positions into the pCDNA.3.1-mPiezo1 plasmid using High-Fidelity DNA Assembly (New England Biolabs). The presence of cpGFP inserts was confirmed by Sanger sequencing (GENEWIZ). The pCDNA3.1-jRGECO1a plasmid was obtained from a previous study (*71*). The double mutants M2241R-R2482H and L2475I-V2476I were inserted into pCDNA3.1-mPiezo1-cpGFP86 and pCDNA3.1-mPiezo1-cpGFP1591 using High-Fidelity DNA Assembly. Plasmids pCDNA3.1-mPiezo1-A2328C/P2382C and pCDNA3.1-mPiezo1-R1762C/E2257C carrying cysteine mutations were generously gifted by Dr. Jorg Grandl (Duke University). To insert these mutations into pCDNA3.1-mPiezo1-cpGFP86, we gel-purified a cpGFP86-containing DNA insert after digesting pCDNA3.1-mPiezo1-cpGFP86 with EcoR1 and XbaI. DNA vectors containing the cysteine mutations were gel-purified after digesting pCDNA3.1-mPiezo1-A2328C/P2382C and pCDNA3.1-mPiezo1-R1762C/E2257C plasmids with EcoRI and XbaI. The cpGFP86-containing insert was then ligated into each cysteine mutations-containing vector. A similar approach was used to insert cysteine mutations into cpGFP1591 except that all plasmids were digested with Acc65I.

Cell culture and transfection

HEK293T cells were obtained from the American Tissue Culture Collection and HEK293$^{\Delta PZ1}$ cells were a gift from Dr. Patapoutian, Scripps Research. Cells were cultured in standard conditions (37 °C, 5 % CO_2) in a Dulbecco's Modified Eagle's Medium supplemented with Penicillin (100 U mL^{-1}), streptomycin (0.1 mg mL^{-1}), 10 % sterile Fetal Bovine Serum, 1X Minimum Essential Medium non-essential amino-acids and without L-glutamine. All cell culture products were purchased from Sigma-Aldrich. Plasmids were transfected in cells (passage number < 35) seeded in 96-well plates at ~50 % confluence 2-4 days before the experiment with FuGene6 (Promega) or Lipofectamine 2000/3000 following the manufacturer's instructions. 1-2 days before experiments, cells were gently detached by 5 min incubation with Phosphate Buffer Saline and re-seeded onto 18 mm round glass coverslips (Warner Instruments) coated with Matrigel (Corning) or onto single or six-channels microfluidic devices (Ibidi µ-slides VI 0.4 or µ-slides I 0.4).

Fluorescence imaging

Excitation light of specific colors were produced by a Light Emitting Diode light engine (Spectra X, Lumencor), cleaned through individual single-band excitation filters (Semrock) and sent to the illumination port of an inverted fluorescence microscope (IX73, Olympus) by a liquid guide light. Excitation light was reflected onto the backfocal plane of a plan super apochromatic 100X oil-immersion objective with 1.4 numerical aperture (Olympus) using a triple-band dichroic mirror (FF403/497/574, Semrock). Emission light was filtered through a triple-band emission filter (FF01-433/517/613, Semrock) and sent through beam-splitting optics (W-View Gemini, Hamamatsu). Split and

bioRxiv preprint doi: https://doi.org/10.1101/2022.06.23.497409; this version posted June 25, 2022. The copyright holder for this preprint (which was not certified by peer review) is the author/funder, who has granted bioRxiv a license to display the preprint in perpetuity. It is made available under aCC-BY-NC-ND 4.0 International license.

unsplit fluorescence images were collected by a sCMOS camera (Zyla 4.2, ANDOR, Oxford Instruments). Spectral separation by the Gemini was done using flat imaging dichroic mirrors and appropriate emission filters (Semrock). Images were collected by the Solis software (ANDOR, Oxford Instruments) at a rate of 1 or 10 frames/second (poking experiments) through a 10-tap camera link computer interface. Image acquisition and sample illumination were synchronized using TTL triggers digitally generated by the Clampex software (Molecular Devices). To reduce light-induced bleaching, samples were pulse-illuminated 200 ms per frame during acquisition. To reduce auto-fluorescence, the cell culture medium was replaced with HBSS approximately 20 min prior experiments.

Image analysis

The first frame of each video was initially pre-processed in ImageJ by manually drawing individual cell boundaries and cropping out all background pixels. This processed image was then used as a guideline to define each cell as a region of interest in $\Delta F/F_0$ analysis. An inhouse MATLAB script was used to determine the average intensity of all pixels associated with each cell.

Cell indentation

Premium standard wall borosilicate capillaries 1.5mm x 4 in (Warner Instruments) were heat-pulled on a horizontal puller (Sutter P-97) and fire-polished on a microforge (Narishige MF-900) to produce smooth and round poking probes with tip diameter 2-5 µm. Poking probes were directly mounted onto a closed-loop piezoelectric actuator (LVPZT, Physik Instrumente) attached to a micromanipulator (MP-225, Sutter Instruments). Probes were moved near the surface of cells of interest at an angle of approximately 60° using. Probes were not allowed to contact cells prior experiments. Probes were linearly displaced in their longitudinal axis at a speed of 1 µm ms^{-1} using a LVPZT amplifier (E-625.SR, Physik Instrumente) and external voltage triggers commanded by Clampex.

Hypotonic shocks

During image acquisition, the extracellular recording solution (HBSS) from cultured dishes was replaced with a hypotonic solution containing 5 mM NaCl, 5 mM KCl, 2 mM $MgCl_2$, 1 mM $CaCl_2$, 10 mM HEPES (pH 7.4 with HCl or NaOH) and 10 mM Glucose. The osmolarity of the hypotonic solution (~58 mOsmol L^{-1}) was measured by a micro-sample osmometer (Advanced Instruments Fiske 210).

Fluid shear stress stimulation and calculations

Fluid shear-stress stimulation was done by circulating recording extracellular solutions at various speeds into a µ-slide channel using a Clampex-controlled peristaltic pump (Golander). The average amplitude of wall shear stress τ applied at the cell surface was estimated using the manufacturer's empirical equation relating τ with flow rate Φ for µ-slide channel with 0.4 mm height:

$$\tau = \eta \times 131.6 \times \Phi$$

bioRxiv preprint doi: https://doi.org/10.1101/2022.06.23.497409; this version posted June 25, 2022. The copyright holder for this preprint (which was not certified by peer review) is the author/funder, who has granted bioRxiv a license to display the preprint in perpetuity. It is made available under aCC-BY-NC-ND 4.0 International license.

Drug treatment

The design of Ibidi μ-slide chambers constrains the diffusion of drugs, which can only be administered through peripheral ports. To ensure sufficient diffusion, cells were treated with each drug 20 min prior to measurement. GsMTx4, Aβ(1–40) and cytochalasin D were administered at a final concentration of 5 μM, 1 μM, and 20 μM, respectively. As GsMTx4 and cytochalasin D are only soluble in DMSO at stock concentrations, pre-treatment introduces a small amount of DMSO to the chambers. Consequently, drug-free controls for GsMTx4 and cytochalasin D were performed by treating cells with 1% DMSO 20 min before measurement. No such treatment was performed for Aβ(1–40), as this peptide is soluble in HBSS at stock concentration. In order to eliminate the possibility of peptide washout following the application of shear stress, HBSS in the pump tubing was also pre-treated with a final concentration of 1 μM Aβ(1–40).

Statistical analyses

All statistical analyses were performed on GraphPad Prism 9.0. Non-parametric Mann-Whitney U-tests (single pairwise comparison) and Kruskal-Wallis test with Dunn's post-correction for multiple comparisons were used to evaluate statistical significance. Exact p-values are provided are provided in all cases, $p < 0.05$ is considered statistically significant for discussion purposes.

bioRxiv preprint doi: https://doi.org/10.1101/2022.06.23.497409; this version posted June 25, 2022. The copyright holder for this preprint (which was not certified by peer review) is the author/funder, who has granted bioRxiv a license to display the preprint in perpetuity. It is made available under aCC-BY-NC-ND 4.0 International license.

Acknowledgements

We thank Dr. Jorg Grandl (Duke University) for generously proving plasmids encoding mouse Piezo1 cysteine mutants. This work was supported by NIH grant GM130834 to J.J.L.

Author contributions

J.J.L. conceived the project; A.D.O., T.W., T.G, A.T., R.G. and J.C. performed experiments. A.D.O., T.W. and J.J.L. analyzed data; J.J.L. and A.D.O. wrote the manuscript.

bioRxiv preprint doi: https://doi.org/10.1101/2022.06.23.497409; this version posted June 25, 2022. The copyright holder for this preprint (which was not certified by peer review) is the author/funder, who has granted bioRxiv a license to display the preprint in perpetuity. It is made available under aCC-BY-NC-ND 4.0 International license.

References

1. D. Choi *et al.*, Piezo1 incorporates mechanical force signals into the genetic program that governs lymphatic valve development and maintenance. *JCI Insight* **4**, (2019).
2. K. Nonomura *et al.*, Mechanically activated ion channel PIEZO1 is required for lymphatic valve formation. *Proc. Natl. Acad. Sci. U. S. A.*, (2018).
3. W. Z. Zeng *et al.*, PIEZOs mediate neuronal sensing of blood pressure and the baroreceptor reflex. *Science* **362**, 464-467 (2018).
4. L. C. Morley *et al.*, Piezo1 channels are mechanosensors in human fetoplacental endothelial cells. *Mol. Hum. Reprod.* **24**, 510-520 (2018).
5. S. Wang *et al.*, Endothelial cation channel PIEZO1 controls blood pressure by mediating flow-induced ATP release. *J. Clin. Invest.* **126**, 4527-4536 (2016).
6. E. R. Schneider *et al.*, A Cross-Species Analysis Reveals a General Role for Piezo2 in Mechanosensory Specialization of Trigeminal Ganglia from Tactile Specialist Birds. *Cell Rep* **26**, 1979-1987 e1973 (2019).
7. E. R. Schneider *et al.*, Molecular basis of tactile specialization in the duck bill. *Proc. Natl. Acad. Sci. U. S. A.* **114**, 13036-13041 (2017).
8. S. S. Ranade *et al.*, Piezo2 is the major transducer of mechanical forces for touch sensation in mice. *Nature* **516**, 121-125 (2014).
9. S. H. Woo *et al.*, Piezo2 is required for Merkel-cell mechanotransduction. *Nature* **509**, 622-626 (2014).
10. K. Poole, R. Herget, L. Lapatsina, H. D. Ngo, G. R. Lewin, Tuning Piezo ion channels to detect molecular-scale movements relevant for fine touch. *Nat Commun* **5**, 3520 (2014).
11. K. L. Marshall *et al.*, PIEZO2 in sensory neurons and urothelial cells coordinates urination. *Nature*, (2020).
12. K. Nonomura *et al.*, Piezo2 senses airway stretch and mediates lung inflation-induced apnoea. *Nature* **541**, 176-181 (2017).
13. Y. Oh *et al.*, Periphery signals generated by Piezo-mediated stomach stretch and Neuromedin-mediated glucose load regulate the Drosophila brain nutrient sensor. *Neuron* **109**, 1979-1995 e1976 (2021).
14. S. Min *et al.*, Control of feeding by Piezo-mediated gut mechanosensation in Drosophila. *Elife* **10**, (2021).
15. P. Wang, Y. Jia, T. Liu, Y. N. Jan, W. Zhang, Visceral Mechano-sensing Neurons Control Drosophila Feeding by Using Piezo as a Sensor. *Neuron*, (2020).
16. S. A. Gudipaty *et al.*, Mechanical stretch triggers rapid epithelial cell division through Piezo1. *Nature* **543**, 118-121 (2017).
17. F. Jiang *et al.*, The mechanosensitive Piezo1 channel mediates heart mechano-chemo transduction. *Nat Commun* **12**, 869 (2021).
18. A. A. Mahmud *et al.*, Loss of the proprioception and touch sensation channel PIEZO2 in siblings with a progressive form of contractures. *Clin. Genet.*, (2016).
19. D. Florez-Paz, K. K. Bali, R. Kuner, A. Gomis, A critical role for Piezo2 channels in the mechanotransduction of mouse proprioceptive neurons. *Sci. Rep.* **6**, 25923 (2016).
20. S. H. Woo *et al.*, Piezo2 is the principal mechanotransduction channel for proprioception. *Nat. Neurosci.* **18**, 1756-1762 (2015).
21. F. S. Passini *et al.*, Shear-stress sensing by PIEZO1 regulates tendon stiffness in rodents and influences jumping performance in humans. *Nat Biomed Eng*, (2021).
22. R. Nakamichi *et al.*, The mechanosensitive ion channel PIEZO1 is expressed in tendons and regulates physical performance. *Sci. Transl. Med.* **14**, eabj5557 (2022).
23. R. Syeda, Physiology and Pathophysiology of Mechanically Activated PIEZO Channels. *Annu. Rev. Neurosci.* **44**, 383-402 (2021).

bioRxiv preprint doi: https://doi.org/10.1101/2022.06.23.497409; this version posted June 25, 2022. The copyright holder for this preprint (which was not certified by peer review) is the author/funder, who has granted bioRxiv a license to display the preprint in perpetuity. It is made available under aCC-BY-NC-ND 4.0 International license.

24. I. Radin *et al.*, Plant PIEZO homologs modulate vacuole morphology during tip growth. *Science* **373**, 586-590 (2021).
25. J. Li *et al.*, Piezo1 integration of vascular architecture with physiological force. *Nature* **515**, 279-282 (2014).
26. S. S. Ranade *et al.*, Piezo1, a mechanically activated ion channel, is required for vascular development in mice. *Proc. Natl. Acad. Sci. U. S. A.* **111**, 10347-10352 (2014).
27. G. T. Eisenhoffer *et al.*, Crowding induces live cell extrusion to maintain homeostatic cell numbers in epithelia. *Nature* **484**, 546-549 (2012).
28. M. M. Pathak *et al.*, Stretch-activated ion channel Piezo1 directs lineage choice in human neural stem cells. *Proc. Natl. Acad. Sci. U. S. A.* **111**, 16148-16153 (2014).
29. W. Sun *et al.*, The mechanosensitive Piezo1 channel is required for bone formation. *Elife* **8**, (2019).
30. X. Li *et al.*, Stimulation of Piezo1 by mechanical signals promotes bone anabolism. *Elife* **8**, (2019).
31. S. M. Cahalan *et al.*, Piezo1 links mechanical forces to red blood cell volume. *Elife* **4**, (2015).
32. S. Demolombe, F. Duprat, E. Honore, A. Patel, Slower Piezo1 inactivation in dehydrated hereditary stomatocytosis (xerocytosis). *Biophys. J.* **105**, 833-834 (2013).
33. C. Bae, R. Gnanasambandam, C. Nicolai, F. Sachs, P. A. Gottlieb, Xerocytosis is caused by mutations that alter the kinetics of the mechanosensitive channel PIEZO1. *Proc. Natl. Acad. Sci. U. S. A.* **110**, E1162-1168 (2013).
34. S. Wang *et al.*, Adipocyte Piezo1 mediates obesogenic adipogenesis through the FGF1/FGFR1 signaling pathway in mice. *Nat Commun* **11**, 2303 (2020).
35. C. Zhao *et al.*, Mechanosensitive Ion Channel Piezo1 Regulates Diet-Induced Adipose Inflammation and Systemic Insulin Resistance. *Front. Endocrinol. (Lausanne)* **10**, 373 (2019).
36. M. Szczot *et al.*, PIEZO2 mediates injury-induced tactile pain in mice and humans. *Sci. Transl. Med.* **10**, (2018).
37. S. E. Murthy *et al.*, The mechanosensitive ion channel Piezo2 mediates sensitivity to mechanical pain in mice. *Sci. Transl. Med.* **10**, (2018).
38. V. Prato *et al.*, Functional and Molecular Characterization of Mechanoinsensitive "Silent" Nociceptors. *Cell Rep* **21**, 3102-3115 (2017).
39. T. Bai *et al.*, Piezo2: A Candidate Biomarker for Visceral Hypersensitivity in Irritable Bowel Syndrome? *J. Neurogastroenterol. Motil.* **23**, 453-463 (2017).
40. A. E. Dubin *et al.*, Inflammatory signals enhance piezo2-mediated mechanosensitive currents. *Cell Rep* **2**, 511-517 (2012).
41. J. R. Holt *et al.*, Spatiotemporal dynamics of PIEZO1 localization controls keratinocyte migration during wound healing. *Elife* **10**, (2021).
42. Q. Zhao *et al.*, Structure and mechanogating mechanism of the Piezo1 channel. *Nature*, (2018).
43. K. Saotome *et al.*, Structure of the mechanically activated ion channel Piezo1. *Nature* **554**, 481-486 (2018).
44. Y. R. Guo, R. MacKinnon, Structure-based membrane dome mechanism for Piezo mechanosensitivity. *Elife* **6**, (2017).
45. J. Ge *et al.*, Architecture of the mammalian mechanosensitive Piezo1 channel. *Nature* **527**, 64-69 (2015).
46. L. Wang *et al.*, Structure and mechanogating of the mammalian tactile channel PIEZO2. *Nature* **573**, 225-229 (2019).
47. C. D. Cox *et al.*, Removal of the mechanoprotective influence of the cytoskeleton reveals PIEZO1 is gated by bilayer tension. *Nat Commun* **7**, 10366 (2016).
48. A. H. Lewis, J. Grandl, Mechanical sensitivity of Piezo1 ion channels can be tuned by cellular membrane tension. *Elife* **4**, (2015).

bioRxiv preprint doi: https://doi.org/10.1101/2022.06.23.497409; this version posted June 25, 2022. The copyright holder for this preprint (which was not certified by peer review) is the author/funder, who has granted bioRxiv a license to display the preprint in perpetuity. It is made available under aCC-BY-NC-ND 4.0 International license.

49. R. Syeda *et al.*, Piezo1 Channels Are Inherently Mechanosensitive. *Cell Rep* **17**, 1739-1746 (2016).
50. M. Luo, K. K. Y. Ho, Z. Tong, L. Deng, A. P. Liu, Compressive Stress Enhances Invasive Phenotype of Cancer Cells via Piezo1 Activation. *BioRxiv*, (2019).
51. J. Xu *et al.*, GPR68 Senses Flow and Is Essential for Vascular Physiology. *Cell* **173**, 762-775 e716 (2018).
52. D. Jetta, P. A. Gottlieb, D. Verma, F. Sachs, S. Z. Hua, Shear stress-induced nuclear shrinkage through activation of Piezo1 channels in epithelial cells. *J. Cell Sci.* **132**, (2019).
53. M. M. Maneshi, L. Ziegler, F. Sachs, S. Z. Hua, P. A. Gottlieb, Enantiomeric Abeta peptides inhibit the fluid shear stress response of PIEZO1. *Sci. Rep.* **8**, 14267 (2018).
54. K. L. Ellefsen *et al.*, Myosin-II Mediated Traction Forces Evoke Localized Piezol Ca2+ Flickers. *Biophys. J.* **116**, 377a-377a (2019).
55. J. J. Lacroix, W. M. Botello-Smith, Y. Luo, Probing the gating mechanism of the mechanosensitive channel Piezo1 with the small molecule Yoda1. *Nature Communications* **9**, 2029 (2018).
56. P. A. Gottlieb, C. Bae, F. Sachs, Gating the mechanical channel Piezo1: a comparison between whole-cell and patch recording. *Channels (Austin)* **6**, 282-289 (2012).
57. M. R. Servin-Vences, M. Moroni, G. R. Lewin, K. Poole, Direct measurement of TRPV4 and PIEZO1 activity reveals multiple mechanotransduction pathways in chondrocytes. *Elife* **6**, (2017).
58. B. Coste *et al.*, Piezo proteins are pore-forming subunits of mechanically activated channels. *Nature* **483**, 176-181 (2012).
59. Y. C. Lin *et al.*, Force-induced conformational changes in PIEZO1. *Nature* **573**, 230-234 (2019).
60. X. Yang *et al.*, Structure deformation and curvature sensing of PIEZO1 in lipid membranes. *Nature*, (2022).
61. D. De Vecchis, D. J. Beech, A. C. Kalli, Molecular dynamics simulations of Piezo1 channel opening by increases in membrane tension. *Biophys. J.* **120**, 1510-1521 (2021).
62. W. Jiang *et al.*, Crowding-induced opening of the mechanosensitive Piezo1 channel in silico. *Communications Biology* **4**, 84 (2021).
63. B. Coste *et al.*, Piezo1 ion channel pore properties are dictated by C-terminal region. *Nat Commun* **6**, 7223 (2015).
64. Q. Zhao *et al.*, Structure and mechanogating mechanism of the Piezo1 channel. *Nature* **554**, 487-492 (2018).
65. F. J. Taberner *et al.*, Structure-guided examination of the mechanogating mechanism of PIEZO2. *Proc. Natl. Acad. Sci. U. S. A.*, (2019).
66. A. H. Lewis, J. Grandl, Inactivation Kinetics and Mechanical Gating of Piezo1 Ion Channels Depend on Subdomains within the Cap. *Cell Rep* **30**, 870-880 e872 (2020).
67. J. Wu, R. Goyal, J. Grandl, Localized force application reveals mechanically sensitive domains of Piezo1. *Nat Commun* **7**, 12939 (2016).
68. J. Cowgill, B. Chanda, The contribution of voltage clamp fluorometry to the understanding of channel and transporter mechanisms. *J. Gen. Physiol.* **151**, 1163-1172 (2019).
69. M. Wulf, S. A. Pless, High-Sensitivity Fluorometry to Resolve Ion Channel Conformational Dynamics. *Cell Rep* **22**, 1615-1626 (2018).
70. Y. Nasu, Y. Shen, L. Kramer, R. E. Campbell, Structure- and mechanism-guided design of single fluorescent protein-based biosensors. *Nat. Chem. Biol.* **17**, 509-518 (2021).
71. A. D. Ozkan *et al.*, Mechanical and chemical activation of GPR68 probed with a genetically encoded fluorescent reporter. *J. Cell Sci.* **134**, (2021).
72. T. Patriarchi *et al.*, Ultrafast neuronal imaging of dopamine dynamics with designed genetically encoded sensors. *Science* **360**, (2018).
73. C. Dong *et al.*, Psychedelic-inspired drug discovery using an engineered biosensor. *Cell*, (2021).

bioRxiv preprint doi: https://doi.org/10.1101/2022.06.23.497409; this version posted June 25, 2022. The copyright holder for this preprint (which was not certified by peer review) is the author/funder, who has granted bioRxiv a license to display the preprint in perpetuity. It is made available under aCC-BY-NC-ND 4.0 International license.

74. S. Chamberland *et al.*, Fast two-photon imaging of subcellular voltage dynamics in neuronal tissue with genetically encoded indicators. *Elife* **6**, (2017).
75. A. Dong *et al.*, A fluorescent sensor for spatiotemporally resolved imaging of endocannabinoid dynamics in vivo. *Nat. Biotechnol.*, (2021).
76. F. St-Pierre *et al.*, High-fidelity optical reporting of neuronal electrical activity with an ultrafast fluorescent voltage sensor. *Nat. Neurosci.* **17**, 884-889 (2014).
77. Y. Wang *et al.*, A lever-like transduction pathway for long-distance chemical- and mechano-gating of the mechanosensitive Piezo1 channel. *Nat Commun* **9**, 1300 (2018).
78. V. Lukacs *et al.*, Impaired PIEZO1 function in patients with a novel autosomal recessive congenital lymphatic dysplasia. *Nat Commun* **6**, 8329 (2015).
79. R. Syeda *et al.*, Chemical activation of the mechanotransduction channel Piezo1. *Elife* **4**, (2015).
80. H. Dana *et al.*, Sensitive red protein calcium indicators for imaging neural activity. *Elife* **5**, (2016).
81. A. H. Lewis, J. Grandl, Stretch and poke stimulation for characterizing mechanically activated ion channels. *Methods Enzymol.* **654**, 225-253 (2021).
82. X. Bao, C. Lu, J. A. Frangos, Temporal gradient in shear but not steady shear stress induces PDGF-A and MCP-1 expression in endothelial cells: role of NO, NF kappa B, and egr-1. *Arterioscler. Thromb. Vasc. Biol.* **19**, 996-1003 (1999).
83. B. Coste *et al.*, Piezo1 and Piezo2 are essential components of distinct mechanically activated cation channels. *Science* **330**, 55-60 (2010).
84. I. Andolfo *et al.*, Multiple clinical forms of dehydrated hereditary stomatocytosis arise from mutations in PIEZO1. *Blood* **121**, 3925-3935, S3921-3912 (2013).
85. W. Zheng, E. O. Gracheva, S. N. Bagriantsev, A hydrophobic gate in the inner pore helix is the major determinant of inactivation in mechanosensitive Piezo channels. *Elife* **8**, (2019).
86. C. Bae, F. Sachs, P. A. Gottlieb, The mechanosensitive ion channel Piezo1 is inhibited by the peptide GsMTx4. *Biochemistry* **50**, 6295-6300 (2011).
87. Jing Wang, Jinghui Jiang, Xuzhong Yang, Li Wang, B. Xiao, Tethering Piezo channels to the actin cytoskeleton for mechanogating via the E-cadherin-β-catenin mechanotransduction complex. *BioRxiv*, (2020).
88. E. D. Nosyreva, D. Thompson, R. Syeda, Identification and functional characterization of the Piezo1 channel pore domain. *J. Biol. Chem.*, (2020).
89. R. Gnanasambandam *et al.*, GsMTx4: Mechanism of Inhibiting Mechanosensitive Ion Channels. *Biophys. J.* **112**, 31-45 (2017).
90. J. Jumper *et al.*, Highly accurate protein structure prediction with AlphaFold. *Nature* **596**, 583-589 (2021).